CrossMark

A Study on Reactive Spray Deposition Technology Processing Parameters in the Context of Pt Nanoparticle Formation

Justin M. Roller and Radenka Maric

Catalytic materials are complex systems in which achieving the desired properties (i.e., activity, selectivity and stability) depends on exploiting the many degrees of freedom in surface and bulk composition, geometry, and defects. Flame aerosol synthesis is a process for producing nanoparticles with ample processing parameter space to tune the desired properties. Flame dynamics inside the reactor are determined by the input process variables such as solubility of precursor in the fuel; solvent boiling point; reactant flow rate and concentration; flow rates of air, fuel and the carrier gas; and the burner geometry. In this study, the processing parameters for reactive spray deposition technology, a flame-based synthesis method, are systematically evaluated to understand the residence times, reactant mixing, and temperature profiles of flames used in the synthesis of Pt nanoparticles. This provides a framework for further study and modeling. The flame temperature and length are also studied as a function of O_2 and fuel flow rates.

1. Introduction

1.1 Catalyst Design by Flame Synthesis

Developing scalable fabrication processes that provide the necessary control of nanoparticle structure for enhanced activity presents significant techno-economic challenges in bringing nanoparticles to large-scale industrial catalytic applications. Flame technology is a scalable and continuous nanoparticle synthesis process and a well-established method for the large-scale production of amorphous carbon, silica and titania (Ref 1). A number of recent reviews explore the wide range of catalytic materials, with properties tailored by the flame processing

Justin M. Roller, Department of Materials Science and Engineering, University of Connecticut, 191 Auditorium Road, Storrs, CT 06269 and Center for Clean Energy Engineering, University of Connecticut, 44 Weaver Rd., Storrs, CT 06269; and **Radenka Maric**, Department of Materials Science and Engineering, University of Connecticut, 191 Auditorium Road, Storrs, CT 06269; Center for Clean Energy Engineering, University of Connecticut, 44 Weaver Rd., Storrs, CT 06269; and Department of Chemical & Biomolecular Engineering, University of Connecticut, Storrs, CT 06269. Contact e-mails: justin.roller@engr.uconn.edu and maric@engr.uconn.edu.

conditions, synthesized by this emerging technology (Ref 2-8).

Results from Roller et al. using reactive spray deposition technology (RSDT), a flame-based method, for Pt-based electrocatalysts clearly have shown that the process can deposit metallic nanoparticle diameters directly onto Nafion® membranes with thin-film thickness' from ~100 nm for unsupported Pt to 10 µm for carbon-supported Pt (Ref 9, 10). The residence time in the flame allows for chemical conversion (homogeneous and heterogeneous) from precursor to monomers, coagulation and coalescence of Pt nanoparticles, and deposition of particles driven by thermophoresis and diffusion (Ref 11). The flame spray synthesis of nanoparticles relies on combustion of a fuel and oxidant as a thermal energy source that drives the conversion of precursor into Pt. RSDT provides adjustable process variables such as flame temperature, stoichiometry, residence time, and downstream quenching rates that couple with solvent and metal precursor concentrations to affect particle: nucleation, growth, annealing, and oxidation.

Recent work by Pratsinis et al. has shown that flame spray pyrolysis (FSP) can be controlled in part to form structured catalyst nanoparticles including Pt and carbon-supported Pt (Ref 7, 4, 12-14). Laine et al. have developed hydrocarbon/NO oxidation catalysts prepared by liquid-feed flame spray pyrolysis (LF-FSP) (Ref 15). Skandan et al. have used a flat flame burner in a vacuum to deposit nanostructured oxide films and powders using the low-pressure flame deposition (LPFD) process (Ref 16). Hunt et al. have disclosed the use of chemical combustion vapor deposition (CCVD) to deposit Pt and carbon-supported Pt films (Ref 17, 18). Choi et al. use an acetylene-air diffusion flame to co-create and deposit carbon-supported Pt powders (Ref 19).

The RSDT process shares the following common properties with flame-based synthesis methods such as CCVD, FSP, LF-FSP, and acetylene-air diffusion flame (Ref 19): they take place in the open atmosphere, use a co-flow turbulent diffusion flame, eliminate the need to dispose of solvent waste, and form the catalyst under dry conditions. Unlike RSDT, LPFD requires a vacuum and uses a flat flame burner in a stagnation-flow configuration. In LF-FSP, the metal precursor is aerosolized with O_2 and ignited with a methane torch in a quartz chamber. With CCVD, the process shares the demonstrated benefit that catalyst production is combined with electrode formation into one step (Ref 20). CCVD and RSDT are the only open atmosphere flame processes that have been used to deposit Pt directly onto a substrate. CCVD used carbon-based gas diffusion layers (GCL) as the substrate, while RSDT uses both the polymeric electrolyte membrane and the GDL.

The RSDT process differs from the CCVD process by the nozzle geometry, processing parameters, and method of injecting the support material (Ref 21). The difference with FSP is the nozzle geometry, atomization mechanism, and the decoupled injection of the support material. The main differences between air-acetylene diffusion flame and RSDT are that the acetylene-air diffusion uses a co-flow pre-mixed geometry, the precursor is atomized by a nebulizer prior to being fed to the burner, and that the enthalpy for precursor conversion is provided primarily by acetylene and not the solvent. The acetylene-oxygen flame is also substantially hotter than a xylene-oxygen flame (3087 versus ~2000 °C).

Due to the relatively few studies involving flame deposition of catalytic particles, using a one-step direct deposition, directly onto polymeric substrates (i.e., Nafion® for fuel cells and solid polymer electrolysis), a systematic study of the fundamental process parameters is warranted. This article focuses on understanding the relationship between processing conditions such as fuel and oxidant flow rates to easily measureable flame properties than may then be used as the basis for further study or as feedback for process control. RSDT Process parameters were selected from conditions used in producing controlled size (2-3 nm) Pt particles (Ref 9, 10, 22). A detailed breakdown of the key process input parameters for producing nanoparticles using flame processing is tabulated in Table 1 and is based on (Ref 3, 6).

1.2 Reactive Spray Deposition Technology

Figure 1(a) shows a diagram of the RSDT process and the three zones of the atomizing burner consisting of (i) solution heating by induction, (ii) co-flow injection of fuel/O_2 and subsequent mixing, and finally (iii) combustion by the pilot flames). Figure 1(b) and (c) show the flame taken with two exposure times under different processing conditions to highlight the time-averaged (Fig. 1b, 1s exposure) and transient properties of a flame (40 ms exposure, Fig. 1c). The RSDT process for platinum particle formation uses a ternary solvent mixture comprising acetone, xylene, and propane as the fuel (Supplementary infor-

mation S1). In the RSDT process, 2,4-pentanedione platinum(II), also commonly referred to as platinum(II) acetylacetonate or Pt(acac)$_2$, is dissolved into xylene and acetone, placed in a sealed vessel, and further diluted with liquefied propane (Supplementary information S1). The precursor solution is then pumped using a high-pressure syringe pump into a custom-made atomizing combustor (Ref 11, 22).

The fuel enters the nozzle through a tube and is heated. To create a pressure drop, the fuel then enters a smaller diameter hypodermic needle. Finally, the solution is atomized at the exit orifice, of the needle, as shown in Fig. 1(b). Using a co-flow design for fuel/O_2 injection, the O_2 is metered. The velocity differential between the fuel droplets and O_2 provides a mixing with the fuel-rich core in the axial spray prior to ignition (Ref 6, 23). Heat, pressure drop, and propane expansion determine the droplet size distribution produced by the atomizing combustor (Ref 24).

The droplets are then ignited by a ring of pilot burners. After ignition, the chosen fuel and O_2 flow settings create conditions that form a jet-diffusion flame with varied degrees of turbulence. The turbulence increases the reactant mixing which increases with higher flows of fuel and O_2 (Ref 6, 25).

After precipitation from droplet evaporation, the precursor then is decomposed to Pt vapor (Ref 3, 26). Nucleation of Pt nanoparticles occurs from this vapor followed by growth of the primary particle along the length of the hot reactive zone (Ref 11, 27-29). Vapors of Pt will begin to nucleate as a function of lateral and radial distances in the flame and the integrated heat absorbed as a function of the flame's thermal profile. The exact location will vary due to processing conditions with larger fuel flow rates and optimal oxidant flow rates leading to hotter and shorter flames with better mixing. Higher temperatures and particle concentrations favor coagulation and sintering of the particles and, thus, favor larger primary particle sizes (Ref 30).

2. Experimental

The following experimental tests were performed for this study: (i) calculation of the basic fluid dynamic properties for the fuel and oxidant flows (based on typical deposition conditions) using the RSDT system, (ii) the droplet size distribution (using laser light scattering) of the fuel feedstock as a function of nozzle temperature, (iii) determination of the geometrical flame shape (estimated from the radiance) and the resultant temperature (at a fixed distance) as a function of fuel and oxidant flow rates, (iv) measurements of the radial and axial temperatures of various flames as a function of the oxidant and fuel flow rates, (v) velocity profiles of the oxidant and estimated residence times based on thin-wire anemometry, and (vi) exit velocity profiles of the fuel with estimated residence times based on volume flow rates through the RSDT nozzle. To simplify this study, quenching air on the flame was turned off.

Table 1 Chemical and physical process parameters for synthesis of Pt by RSDT

	Species	Unit	Range	Effects
Chemical inputs				
Solvent	Xylene, acetone, propane	wt.%	Xylene: 40-60%, Acetone: 15-30% , Propane: 15-25%	Solubility of precursor, atomization (droplet size, distribution, and velocity), temperature of flame (i.e, enthalpy of combustion), combustion dynamics
Precursor	Pt(II)-acetylacetonate	Molarity, M	0.001-0.02 M	Solubility, decomposition temperature, location of vaporization in flame, tendency to foul the burner, cost
Oxidant	Oxygen	wt.%	21-100%	Equivalence ratio, cost, oxidizing strength of flame and temperature of flame
Pilots	Oxygen and methane	wt.%	30-50% CH$_4$	Ignition point, temperature of the exit orifice, and tendency for fouling
Quench	Dry air	wt.%	100%	Rate of cooling and cost
Physical inputs				
Solvent flow rate	Xylene, acetone, propane	L/min	0.003-0.006 L/min	Metal flux, pressure drop in burner, droplet size, length of flame, temperature of solvent, droplet lifetime, and substrate temperature
Oxidant flow rate	Oxygen	L/min	0-13 L/min	Equivalence ratio, temperature of flame, turbulence of flame, shaping of spray angle, air-to-liquid ratio, flame velocity, evaporation rate, and atomization
Pilots	Oxygen and methane	L/min	0.6-1.2 L/min	Ignition point, temperature of the exit orifice, and tendency for fouling
Quench	Dry air	L/min	0-100 L/min	Crystallinity, substrate temperature, phase, entrained air, momentum to direct secondary spray at substrate, mixing and deposition efficiency

2.1 Flame-Based Deposition System

Process analysis for the RSDT system was performed on a custom-made deposition system that consists of the following sub-systems: Isco 500D syringe pump and precursor reservoir (Teledyne Isco, Lincoln NE); EasyHeat 0112 (Ameritherm, Scottsville, NY) induction heating power supply with custom helical coil; custom-made atomizing burner (Ref 10, 22); and a linear 3-axis servo-driven motion system to sweep the substrate across the deposition zone (Techno Isel, New Hyde Park, NY). The heating stage of the process comprises a 316 stainless steel tube (Cadence Science, Cranston RI) that has an outer diameter of 0.159 cm, which is 10 cm in length, and has an inner diameter of 0.25 mm. The tube was heated by induction using a custom 7 loop helical coil that spans the entrance port at tube 1 to the end of the heating zone. The control point for monitoring the process temperature was located 9.9 cm from the entry of the tube and set to a value of 190 °C. Soldered to the end of the tube is a 32 gage hypodermic insert (length of 1.8 cm and an inner diameter of 100 μm) that acts as the fuel exit orifice. The hypodermic also functions as a flow restrictor to induce a fast pressure drop just prior to exit into the atomizing/ mixing zone.

2.2 Atomizing Burner

Details of the process are described in references (Ref 10, 22). A detailed view of the RSDT atomizing nozzle is shown in Fig. 2. The process streams are shown imposed on a close-up view of the atomizing burner in Fig. 2 to further clarify the geometry and dimensions. All volu-metric and mass flow data are calculated based on the dimensions of the nozzle/burner assembly shown in Fig. 2 (Supplementary information S2, S3). The pressure drop of the fuel in the system was measured with a transducer embedded in the head of the syringe pump.

Previous work by Roller et al. (Ref 9, 10) was used as the basis for choosing the fuel composition, precursor, and oxidant flow rates. A typical precursor solution (used in the RSDT process) for synthesis of Pt nanoparticles consists of xylene, acetone, propane, and Pt-acac in the mass proportions listed in Supplementary information S1. Typical pressure drops of ~140 psi are observed at a liquid flow rate of 4 mL/min through the atomizing burner. This restriction prevents the liquid feedstock in the conduit from vaporizing prematurely in the nozzle and precipitating Pt-(acac)$_2$ in tube 2 thereby clogging the flow path. The back pressure is a function of the size of the conduit, flow rate of the fuel, and control point temperature.

Precursor solution was continuously passed through the heating stage at flow rates of 3-6 mL/min. The hypodermic insert is surrounded by a ∅ 0.38 cm concentric channel; the channel supplied 99.8% oxygen (Airgas East Inc., Cheshire CT) as the fuel oxidant as shown in Fig. 2 of reference (Ref 10). O$_2$ was used as the oxidant and passed at flow rates of 2.3 to 9.3 L/min. The length of the atomizing/mixing zone is 0.20-0.38 cm. The ignition zone consists of six circular ports having a ∅ 0.05 cm and angled at 45° to the centerline of the hypodermic needle. The six ports were evenly spaced on a 0.32 cm radius around the hypodermic insert. These ports supply a pre-mixed methane (99.999% Airgas East Inc., Chesire, CT) and O$_2$ stream that is ignited to provide the primary ignition source for droplets exiting hypodermic
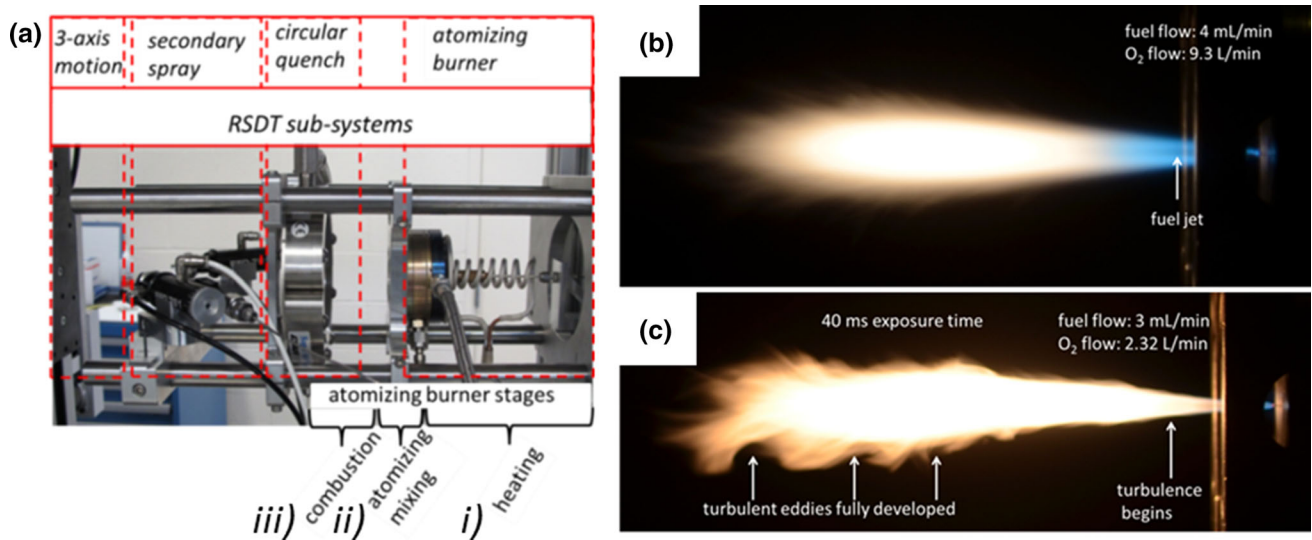
Fig. 1 (a) System configuration of the RSDT hardware highlighting stages in which the Pt catalyst passes during formation. The secondary spray injects the (optional) carbon support. (b) Fuel and oxidant inhomogeneity in the combustion zone such as the central unburned fuel jet and (c) the development of turbulent eddies growing outward from the point of combustion
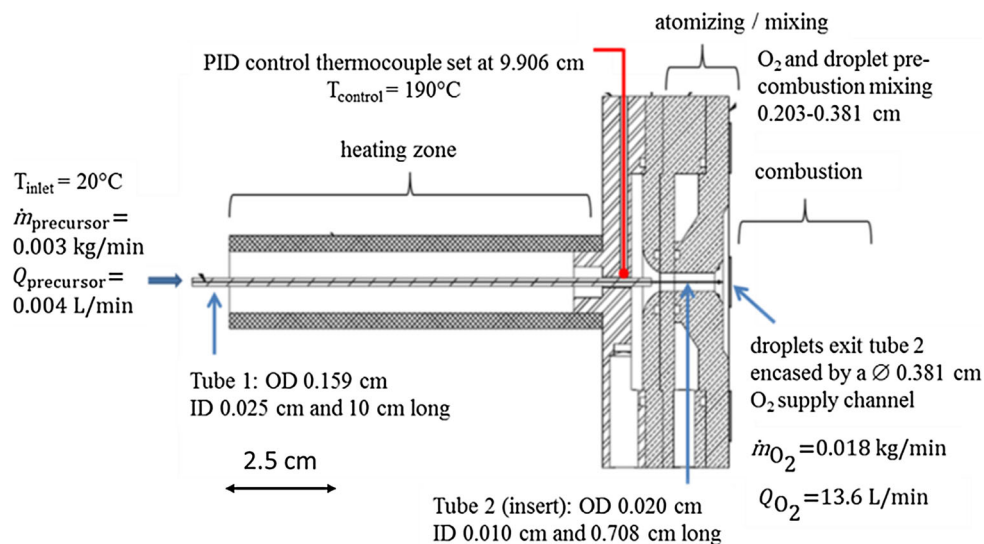

Fig. 2 Expanded view of the atomizing burner showing the entrance and exit of the fluid streams in relation to the heating, atomizing/mixing, and combustion zones for a fuel flow rate of 4 mL/min and an O_2 flow rate of 13.6 L/min

needle. As described in Fig. 2, tube 2 is centered in an opening through which the O_2 is passed in a coaxial geometry; this is shown in Fig. 2 of Roller et al. (Ref 10). The opening of the O_2 supply channel is 0.114 cm², while the tube 2 cross section is only 3.2E−4 cm² (356:1). Mass and volume flow rates for a typical deposition are listed in Supplementary information S2.

2.3 Droplet Size Measurements

In order to better understand the relationship between nozzle temperature, $T_{control}$ (presented in Fig. 2), and the

output droplet size, a series of laser light scattering experiments were performed at a fixed distance of 5 cm from the face of the nozzle (Supplementary information S5). Droplet size measurements were collected on a Malvern Spraytec analyzer with a 632.8 nm, 5 mW helium-neon laser, and a 36 element log-spaced silicon diode detector array. Two different solutions were prepared each containing 54 vol.% xylene, 20 vol.% acetone, and 26 vol.% propane. One of the solutions also had 10 mM of Pt-acac dissolved in the solvent (Supplementary information S1). Plots of the frequency (%) as a function of droplet size are shown in Fig. 4.

2.4 Flame Temperature and Velocity Measurements

Velocity profiles of the oxidant gas along the central spray axis were recorded using a 407123 Extech hot wire thermo-anemometer. The anemometer was mounted to the 3-axis servo-driven motion system, and measurements were taken to 18 cm from the nozzle face. Due to support bracketing for the atomizing burner, the anemometer probe could not be brought closer than ~3.5 cm. In that region, the velocity was estimated by fitting a 2nd-order polynomial to the data between 3.5 and 18 cm and extrapolating to 0 cm. The residence time was determined by integrating the velocity data (Fig. 6a). The residence time was also estimated based on exit velocities of both the fuel and oxidant volumetric flow rates in the nozzle tubes.

The centerline and radial temperature measurements in the flame were made with a 0.5 mm thin-wire Pt-Rh thermocouple (Type B, Omega Engineering) mounted to the 3-axis servo-driven motion system. Data were logged using a custom Lab-View acquisition program.

2.5 Flame Geometry Measurements

Flame images were obtained using Canon EOS 60D DSLR 18 megapixel camera set to an f-number of 36 and a shutter speed of 1 s except as noted. The flames were photographed at 90° to the direction of the nozzle face.

3. Results and Discussion

The discussion and results will follow the order in which the processing steps are sequentially taking place to generate Pt. The order is as follows: (i) pump precursor solution through nozzle, (ii) heat the solution with induction, (iii) pump oxidant through the nozzle, (iv) atomize precursor solution, (v) mix precursor droplets with oxidant, and (vi) ignite the droplet/oxidant mixture.

3.1 Precursor Solution Fluid Dynamics and Ignition Geometry

The precursor solution enters the atomizing burner through tube 1 (Fig. 2) whereby heating from the helical induction coil begins. Residence time of the fuel in the nozzle can be calculated by dividing the internal volume of the cylindrical tube by the volumetric flow rate.

$$\frac{\pi r^3 l}{Q_{\text{fuel}}} = \text{Residence time}, \tag{Eq 1}$$

where r is the tube radius, l is the length of the tube, and Q_{fuel} is the volumetric flow rate. At a flow rate of 4 mL/min, the residence time of the solution in tube 1 is 76 ms (internal volume of tube is ~5 μL), while the residence time in tube 2 is ~2 ms (internal volume ~0.15 μL). The fluid flows in both tubes are fully developed flow, since the $l_{\text{o, tube 1}}/d_{\text{o, tube 1}}$ is 394 while $l_{\text{o, tube 2}}/d_{\text{o, tube 2}}$ is 177, where l_{o} is the length and d_{o} is the diameter (Supplementary

information S3). This gives a velocity of 1.3 m/s in tube 1 and 8.2 m/s in tube 2. Reynolds numbers of 534 and 1341 are found for tubes 1 and 2, respectively indicating laminar flow in these sections of the tube (Supplementary information S3).

In general, the outside of tube 1 (at 10 cm from the entrance port) is heated to 190 °C (indicated as point T_{control} in Fig. 2) with 4 mL/min of precursor solution passing through the system. The outer surface temperature of tube 1 at 3.5 cm from the entrance port is ~40 °C. The temperature of a xylene solution (passing out of the exit orifice of tube (2) and striking a thermocouple is 45 °C. Even though the surface temperature of the tube is set to 190 °C, there is only enough heat transferred (~2 W) to raise the temperature of the fuel to ~25 °C (Supplementary information S7). Raising the control temperature either introduced instabilities in the flow (pulsations), precursor precipitation in the hypodermic tube, or caused premature failure of o-rings sealing the nozzle. One practical way to increase the amount of heat transferred to the solution would be to increase both the length of tube 1 and the induction coil or to decrease the flow rate.

After passing through the heated zone, the solution then enters tube 2 and experiences a rapid acceleration (velocity increases from 1.3 to 8.2 m/s) (Supplementary information S3). Conditions for heat loss occur during this stage since this area is outside the induction zone and there is a large volume of O_2 passing over tube 2 (see Fig. 2, blue arrow labeled as tube 2). The resultant heat loss is a function of two counteracting phenomena, residence time and surface-to-volume ratio of the inner tube. The short residence time in this section (~2 ms) limits heat transfer. However, the surface-to-volume ratio of the tube to solution increases from 157 cm^{-1} in tube 1 to 394 cm^{-1} in tube 2.

After precursor solution exits from the tip of tube 2 (i.e., the exit orifice) and is released into the open atmosphere, there will also be an associated temperature drop due to evaporation and expansion of the propane (Ref 31). The evaporation rate is dependent on temperature, flow differential between the droplets with the supplied O_2, and surface area. Evaporation is not uniform with time since the droplets are decreasing in size which reduces the surface area during travel along the reaction zone. Evaporation occurs when molecules of the liquid droplet have sufficient kinetic energy to overcome liquid-phase intermolecular forces. Evaporation leaves the remaining molecules in the droplet with lower average kinetic energy (i.e., evaporative cooling). Larger initial droplets take longer to evaporate and create more distinct and globular regions of enriched fuel air mixture than for smaller droplet sizes (this nonhomogeneous mixture can result in chaotic combustion) (Ref 32, 33).

It should also be noted that the temperature of the exiting solution can be affected by radiation, due to combustion occurring near the tip, conductive heat transfer from tube 1, and also by the pilot flames as shown in Fig. 3(a) and (b). The flamelets generated by the six pilot burners are angled at 45° to the face normal of the
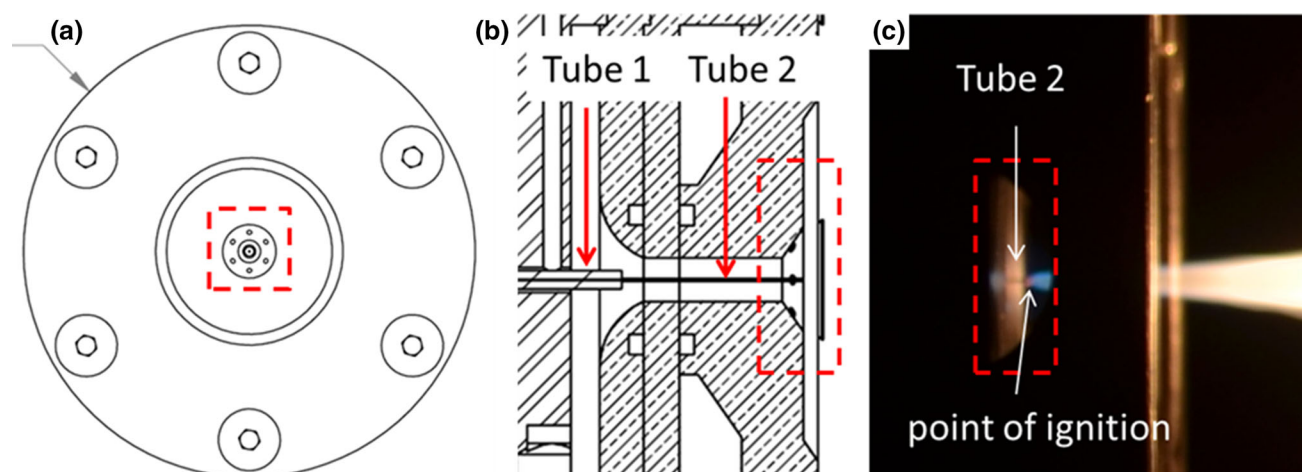
Fig. 3 RSDT combustion nozzle (a) face with pilots, tube 2 and oxygen annulus highlighted. (b) Side view of nozzle showing the transition of tube 1 to tube 2 into the annulus flooded with oxygen and then the six pilot burners angled 45° to the nozzle face (dashed box). (c) Location of tube 2 and point of ignition (view of pilots is obscured by the nozzle holder)

nozzle. Therefore, if the needle is placed too far forward or the ignition gas flow rates are too high, then adverse heating of tube 2 can occur. A slight orange glow can be seen on the tip of tube 2 (Fig. 3c), indicating that substantial heat is being absorbed. Flame pulsations, precursor build-up around the exit orifice, and clogging are symptoms of an overheated exit orifice.

A nozzle design (or set of stable operating conditions) which lifted the ignition point off of the end of tube 2 would extend the service life of each injector, reduce clogging, reduce fouling, and prevent contamination from the steel. This observation suggests that careful consideration of the location of tube 2 in the atomizing burner, flow rate of flamelet gases, angle of flamelet gas injection, and oxidant flow rate can be used to optimize the injection conditions and limit heat transfer from the flames to the injector port. Additionally, incorporation of a swirl-type or low-swirl atomizing combustor may limit fatigue of tube 2, eliminate clogging events, and create a more uniformly mixed flame zone (Ref 34, 35).

3.1.1 Process Parameters Affecting Atomization. Atomization in the RSDT process is affected by the following parameters: (i) physical characteristics of the precursor solution which are a function of temperature, (ii) flow rate of the precursor solution, (iii) flow rate of the oxidant gas, (iv) nucleation rate of the propane bubbles, and (v) velocity differential between the precursor solution and oxidant at the mixing stage.

Viscosity, surface tension, and density are key temperature-dependent parameters that determine the droplet size distribution in sprays (Supplementary information S4). Low viscosity and surface tension favor atomization (Ref 33). As an approximate estimate, the surface tension (at 25 °C) of a mixture of ~62 wt.% xylene and ~21 wt.% acetone and 17 wt.% propane is ~23.6 mN/m with a mass averaged density of 779.9 kg/m^3 (Supplementary information S3, S6). The induction coil heats the solution to ~50 °C decreasing the surface tension and

viscosity by 15-20% for both acetone and xylene (Supplementary information S6). Propane on the other hand experiences a decrease of 36% in viscosity and 60% in surface tension over this temperature range (Supplementary information S6).

The break-up of droplets is further aided by gas evolution caused by the nucleation and growth of propane bubbles in tube 2, see Fig. 1 in (Ref 11). The rate of nucleation density is driven by the degree of superheating and the rapid drop in pressure near the outlet of the nozzle (Ref 36). The compressed gas-phase escapes the mixture, expanding rapidly and shattering the liquid fuel into ligaments and droplets. The estimated velocity of the liquid exiting tube 2 is ~8.2 m/s based on a volume flow rate of 0.004 L/min in a 1.02×10^{-3} cm inner diameter tube (Supplementary information S3). The oxidant velocity is 19.9 m/s creating a velocity differential of 11.7 m/s (Supplementary information S2). This extra oxidant flow (3400:1 by volume) further breaks-up the droplets (by shear force) and reduces the spray angle (Ref 33). The point of fuel ignition is shown in Fig. 3(c).

3.1.2 Droplet Size Measurements. The results of the droplet size measurements (Fig. 4) were interesting in three distinct ways. First was the relative invariance of the droplet size to nozzle temperature. The additional heat added to the fuel by changing the temperature by 100 °C is <1 watt (Supplementary information S7). Second was the relatively large size of the droplets (~14-17 μm) compared to those obtained by Pratsinis et al. (Ref 3, 12). The use of propane in the precursor solution and the inner diameter of the exit tube (tube 2) being 0.1 mm both favor finer atomization. Pratsinis et al., at ETH, have reported a $D_{v,50}$ droplet size of ethanol as between 5 and 25 μm (Ref 3, 12) as a function of oxidant flow rate. Pratsinis et al. do not use heating or propane to aid in atomization and instead use an off-the-shelf external-mixing gas assisted stainless steel nozzle (Schlick-Düsen, Gustav Schlick GmbH, 970/4-S32). The fuel capillary tube has a 0.5-mm
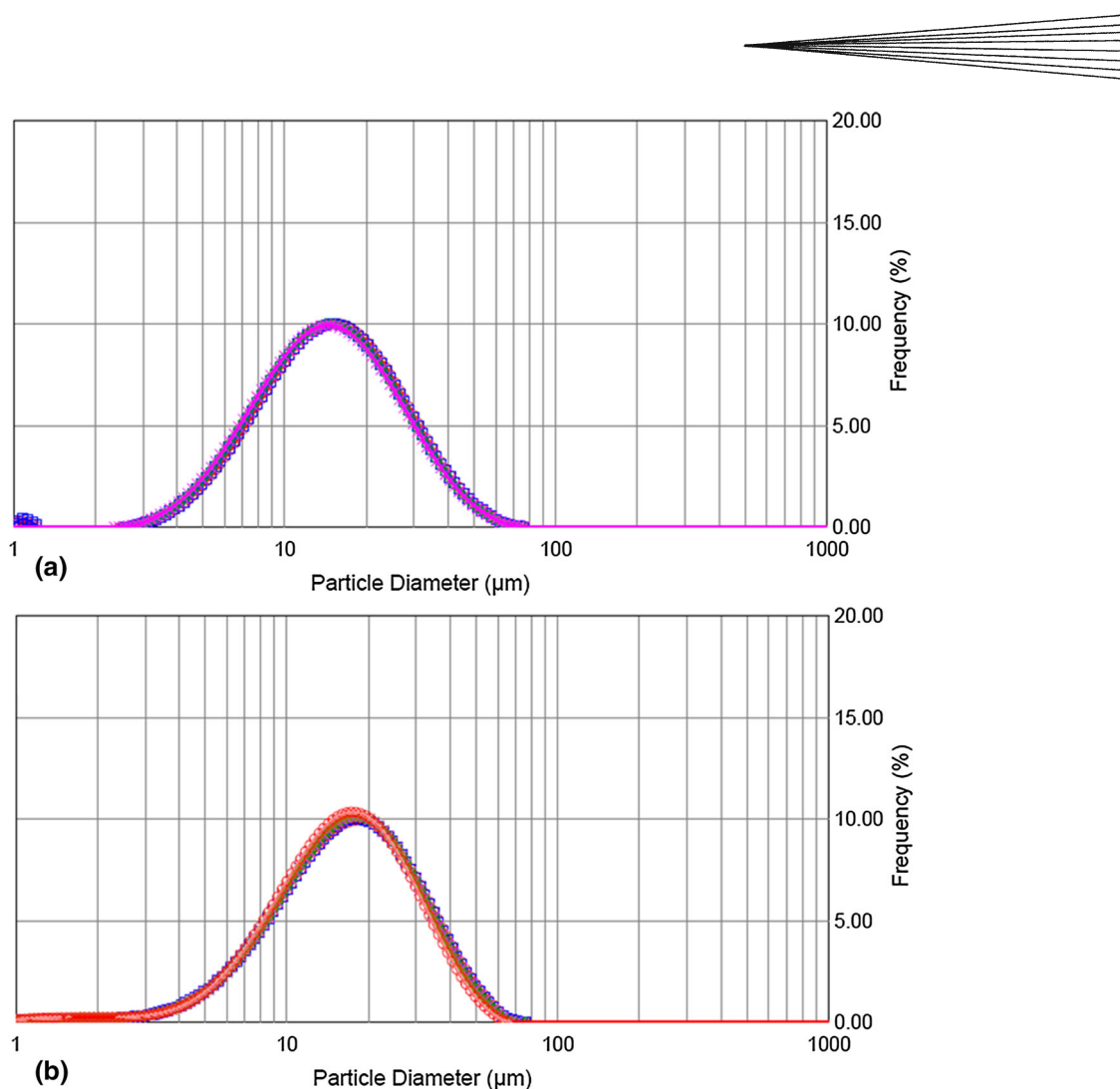
Fig. 4 Droplet size as determined by laser diffraction at a sampling distance of 5 cm from the nozzle face using (a) 54 vol.% xylene, 20 vol.% acetone, and 26 vol.% propane and (b) 54 vol.% xylene, 20 vol.% acetone, 26 vol.% propane and 10 mM of Pt-acac

inner diameter and the tube creates an annular gap that can be adjusted (with a gap area up to 0.48 mm^2) to keep a constant oxygen pressure drop (1 bar) across the nozzle (Ref 3, 12). The FSP process uses a tube diameter at the exit orifice that is ~×4.9 greater than tube 2 yet still maintains an acceptable atomization level. The area created by the annular gap in the FSP process is ~×14 smaller. This empirically suggests that decreasing the area of the annulus between the fuel and O$_2$ flow in the RSDT process would further aid in atomization.

Typical O$_2$ flow rates for FSP (3 L/min) are approximately half of those typically used for RSDT. According to Pratsinis et al., the angle created by the oxidant orifice exit, which is normal to the nozzle face, and the conduit supplying the oxidant play a critical role in creating an effective dispersive force on the injected fuel (Ref 3, 12). In the RSDT process, this angle is 90° (i.e., a straight pipe), whereas in the FSP process, the angle is closer to 45°. However, in FSP, the oxidant flow and atomization appear to be more coupled. Oxidant flow rate has important cost considerations for the system. Oxygen is

more costly than air, and therefore, the ability of a nozzle to generate sufficient atomization with air would substantially reduce process costs.

Third, the droplet sizes were sampled at 5 cm from the atomizing burner face where the interaction of the spray with the laser could be easily observed. However, Fig. 3(c) indicates almost no region between the exit of tube 2 and the start of the flame luminescence, suggesting that a sampling location closer to the ignition point would be more appropriate. The C_v value (Supplementary information S5), an indicator of the droplet density, suggests that increasing the control temperature from 150 to 250 °C results in a decrease in droplet concentration of ~18%, while the droplet diameter is only marginally affected. A value of 2-3 ppm for the C_v indicates a very low concentration of scattering droplets (e.g., 2 ppm is equal to 2 cm^3 of droplets per m^3 of air). Therefore, the spray is rather sparse and the majority of the volume has already evaporated. The result is that only the larger generated droplets remain to be counted and hence skewing the distribution.

3.2 Oxidant/Fuel Velocity and Residence Time

The 3D temperature and velocity field that the precursor metal experiences define the characteristics of the final nanoparticles (Ref 37). The combustion stage should ideally provide a uniform temperature profile that is sufficient for precursor conversion. Additionally, the velocity profile of the reaction zone should be such that there is ample residence time, after metal vapor formation, for the nanoparticle to grow to the desired size and/or crystallinity, see Fig. 1 in (Ref 11). The effects of process parameters on oxidant and fuel velocity are therefore useful to determine boundaries on the residence time.

The calculated exit velocities based on volumetric flow in a tube (Supplementary information S3) for O_2 and fuel (plotted in Fig. 5a and b, respectively) scale linearly with increasing flow rate. The residence time can be estimated by dividing the exit velocity of each stream by an 18 cm distance. This is a common geometry between the nozzle face and substrate (Ref 9, 10). The residence time de-

creases as $1/Q$ where Q is the volumetric flow rate. Residence time, as estimated by this approach, is only an upper limit approximation since expansion of the gases during combustion will further accelerate the gases (Ref 25). The experimentally measured exit velocity (Fig. 6a) and the calculated exit velocity deviate above ~3.71 L/min and this is perhaps due to errors in the extrapolation (see Fig. 5a). The pressure drop created by the fuel flowing in the atomizer was experimentally measured and plotted as a function of fuel flow rates in Fig. 5(b). The exit velocities of the gas and fuel are comparable under the process conditions studied.

In flame aerosol synthesis, product particle size and structure are partially controlled by the particle residence time in the high-temperature region of the flame through the particle sintering and coagulation rate (Ref 38). The estimated velocities of 5-10 ms within oxidant flow rates conducive to mixed flames agree well with values obtained by Gröhn et al. using the flame spray pyrolysis system to
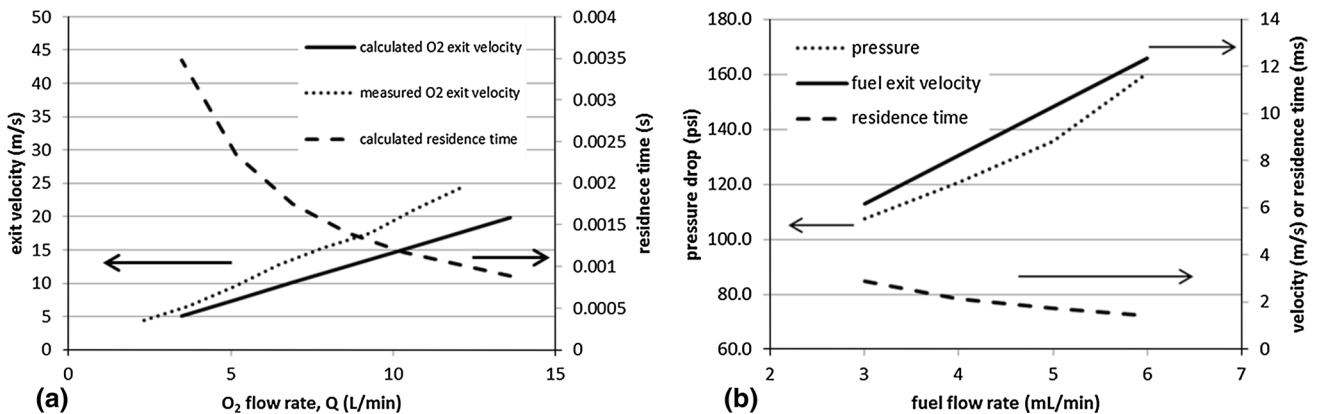

Fig. 5 (a) Exit velocities of the oxidant calculated from the volumetric flow in a tube and the experimentally determined velocity profile. (b) Fuel velocity calculated from the volumetric flow in a tube
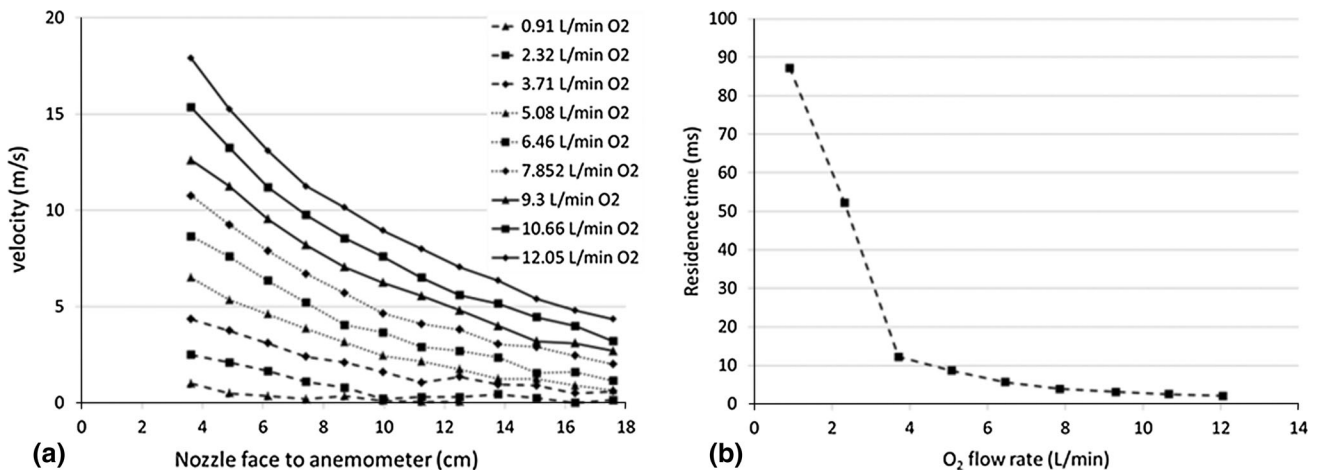

Fig. 6 Velocity profile, recorded by an Extech hot wire anemometer, along the axis (a) extending from centerline of the nozzle and (b) the calculated particle residence time estimated by fitting a 2nd-order polynomial to the data in part A, extrapolating to 0 cm and then integrating
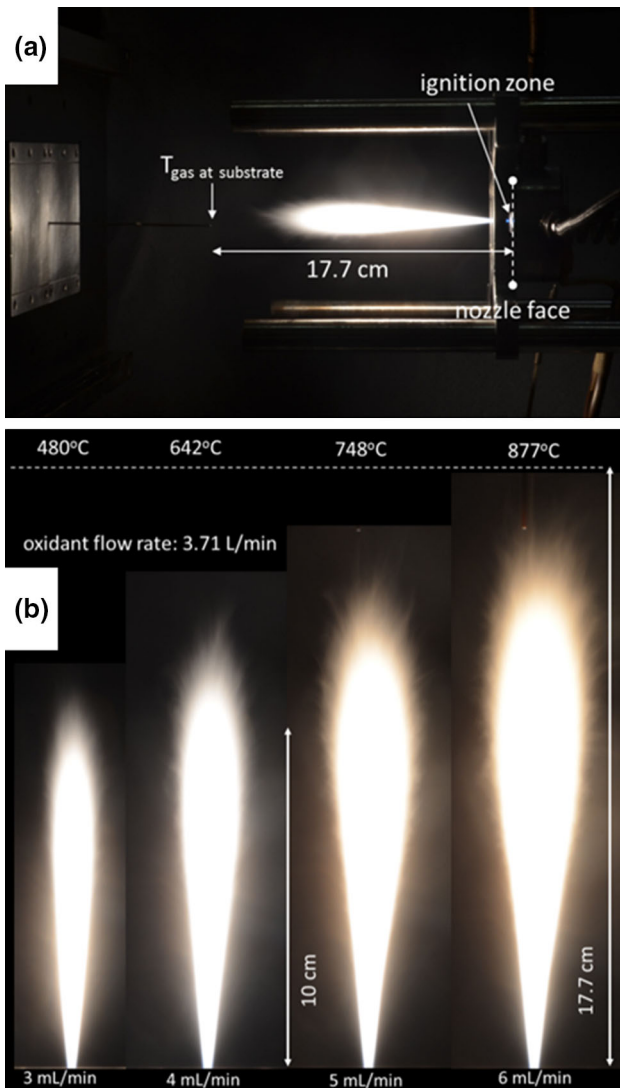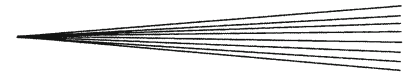
Fig. 7 (a) Experimental set-up for measuring the gas temperature $T_{gas-substrate}$, at a fixed distance of 17.7 cm from the nozzle face and (b) for capturing the geometry of the flame under different fuel flow conditions at a fixed O_2 flow rate of 3.71 L/min

study the formation of ZrO_2 (Ref 38). This suggests that oxidant flow rate can be used as a proxy measure of the residence time.

3.3 Combustion

3.3.1 Gas Temperature at the Substrate Plane. During combustion, fuel vaporizes at the droplet surface and diffuses outward, while oxidizer diffuses inward from the ambient environment. The fuel and oxidizer react stoichiometrically, resulting in a zone of intense reaction. Heat is transported via conduction and radiation outward from the flame and inward back to the droplet surface. The heat deposited at the droplet surface is balanced by the evaporation process at the vapor/liquid interface (Ref 25).

In jet-diffusion flames, a distribution of temperatures exists that vary radially and axially depending on the equivalence ratio, type of fuel, type of oxidant, and transport phenomena resulting from mixing of the droplets with the oxidant (Ref 6, 25). The heat released by combustion is coupled to the degree of mixing between the oxidant and fuel which dictates how the gas flow transfers heat to the substrate. Temperature of the substrate is often a convenient and important process variable to monitor. Figure 7(a) shows the geometry of the thermocouple to the flame and illustrates how the gas temperature ($T_{gas-substrate}$) at the substrate plane was measured. This distance (17.7 cm from the nozzle face) is commonly used in RSDT depositions (Ref 9, 10).

3.3.2 Gas Temperature and Flame Geometry as a Function of Fuel Flow Rate. At a fixed O_2 flow rate, increasing the fuel flow increases $T_{gas-substrate}$ since the flame is longer (Fig. 7b). At a fixed fuel flow rate of 3 or 4 mL/min, increasing the oxidant flow rate from 2 to 4 L/min increases T_g by almost 100 °C. Further increases in the oxidant flow rate decrease T_g. The temperature at the fixed point T_g is a function of the flame length (i.e., proximity to the reactive zone) and the efficiency of the combustion. If there is too much oxidant then the excess acts to increase the flame velocity (i.e., lower particle residence time) and laden the combustion zone with more gas (Ref 25, 39). This excess gas absorbs the generated heat, thus lowering the flame temperature. A combination of lower temperature and shorter residence time favors smaller nanoparticles since coagulation and coalescence are reduced.

3.3.3 Gas Temperature and Flame Geometry as a Function of Oxidant Flow Rate. The flame geometry and gas temperatures as a function of oxidant flow rate are shown in Fig. 8. Two important observations about trends in the RSDT flame are evident. First, the peak in the flame length in Fig. 8(c) (4 mL/min fuel flow) at an O_2 flow of 3.71 L/min also coincides with a thinner flame profile, Fig. 8(a). Increasing the O_2 flow rate to 5.08 mL/min leads to an increase in the width again. Fuel flow rates of 5 and 6 mL/min do not exhibit this peak in flame length or narrowing of the width (Fig. 8d).

The behavior in flame length as a function of oxidant flow has been described by Hawthorne et al. (Ref 39). Initially, the increase in oxidant flow increases mixing of the fuel droplets; the metered oxidant; the entrained ambient air; and the burn rate. When mixing of the fuel and oxidant is slow, compared with the reaction rate, then mixing controls the burning rate. This is the case before 3.71 L/min in Fig. 8(a). This type of burning produces a diffusion flame and its characteristics are defined by how the oxidant and fuel are brought together. Molecular and turbulent diffusions control the mixing and each occurs at different rates (Ref 39). Diffusion flames are characterized by the burning (consumption) rate which in turn is determined by the fluid dynamics of how and where in the process reactants are mixed in the proper ratio for reaction (Ref 40). The burning rate is capped on one extreme by the chemical reaction rate and at the other end by mixing. Figure 8 suggests that near an O_2 flow rate of 3.71
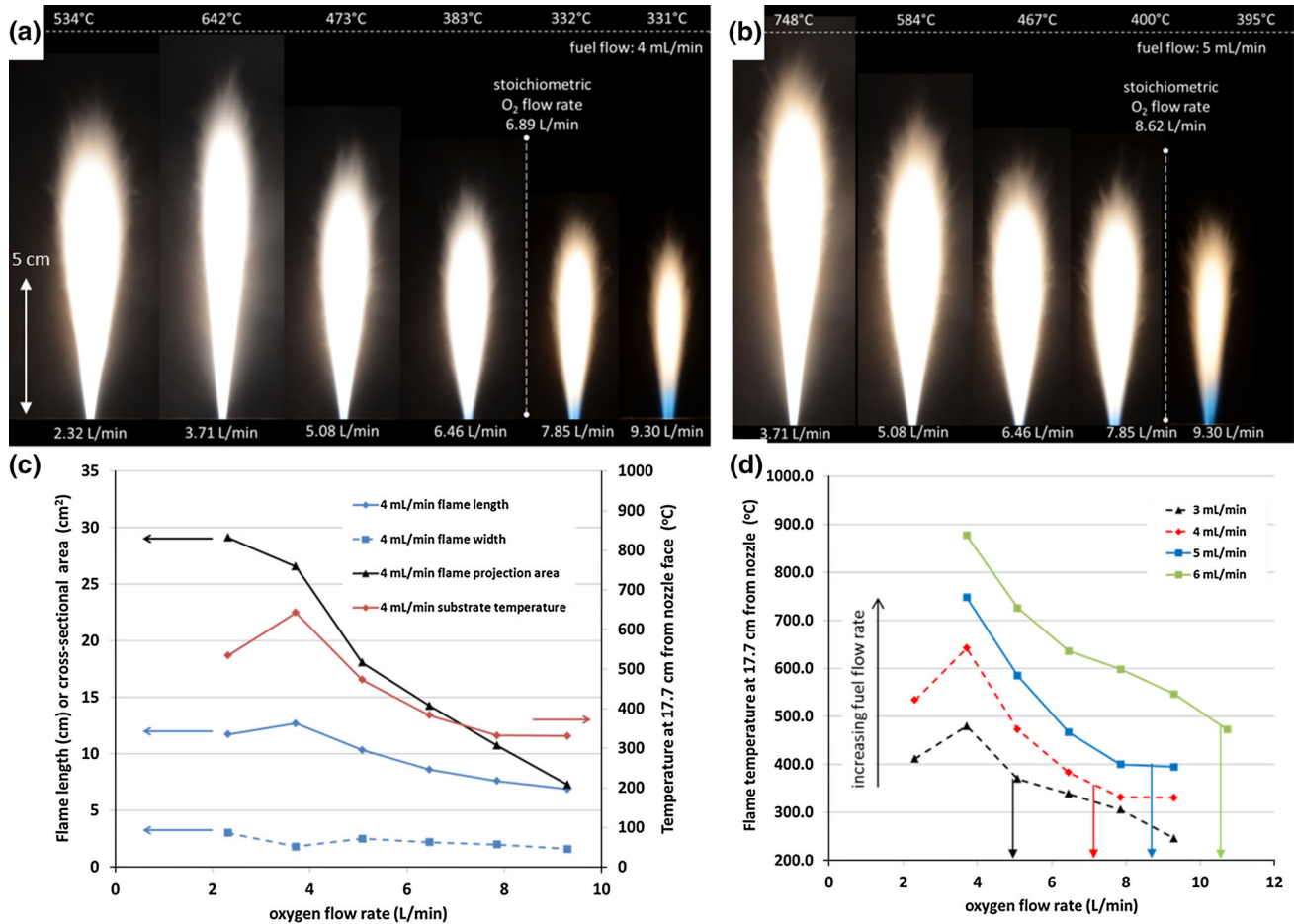
Fig. 8 Profile of several flames at fuel flow rates of (a) 4 mL/min and (b) 5 mL/min at O_2 flow rates between 2.32 and 9.3 L/min. (c) Plots of the flame length, width, projected area, and substrate temperature as a function of O_2 flow rate at a constant fuel flow rate of 4 mL/min (vertical lines indicate stoichiometric O_2 flow rate). (d) Flame geometry under a constant oxidant flow rate with changing fuel flow rates

L/min, the transition from a laminar to turbulent flame begins. As the oxidant flow rate increases, the turbulent mixing zone occupies a larger portion of the flame length.

Note that at 3.71 L/min, the equivalence ratio, ϕ, is 1.81 indicating fuel-rich conditions (Supplementary information S9). The O_2 flow rate is nearly half of the stoichiometric required flow of 6.89 L/min ($\phi = 1$). This indicates that the additional oxidant must be supplied by entrainment from the surrounding air. While an overall stoichiometric value for burning 4 mL/min of the fuel requires 6.89 L/min of O_2, the conditions locally could be fuel lean or rich. This is due to the fact that the droplets are injected into the central axis of the flame and their number density decreases radially and axially along the path of the reaction zone (Ref 41, 42). The O_2 gas expands radially outward from the nozzle exit by convection and diffusion while the spray droplets have a more ballistic component to their velocity (Ref 13). Without a shroud to confine the combustion plume, there is entrainment of the surrounding gases from the atmosphere (Ref 43, 44). Figure 1(b) shows a set of

conditions (fuel lean), whereby the fuel jet extends several centimeters into the flame. The exposure time is 1 s to reveal the time averaged length of the flame. In contrast, Fig. 1(c) shows a 40 ms exposure and this image reveals the growth of turbulent eddies in the flame at very low O_2 flow rates. The flow transitions from laminar to turbulent along the spray axis and this turbulence propagates outward from the point of ignition (Ref 25).

If the mixture is fuel rich, then more particulate matter from the soot is generated and this increases the radiance making visibility of the central fuel core more difficult at lower O_2 flow rates (Ref 45). Flame radiance also increases axially down the combustion flame as more and more particles (i.e., soot and Pt) are generated, see Fig. 1. There is a clear change in the flame color with a concurrent increase in blue radiance, in the area after the point of ignition, when crossing the stoichiometric boundary (indicated by the vertical broken line in Fig. 8a and b). The bluish color is attributed to the chemiluminescent emissions from excited states of CH, OH, and C_2 species
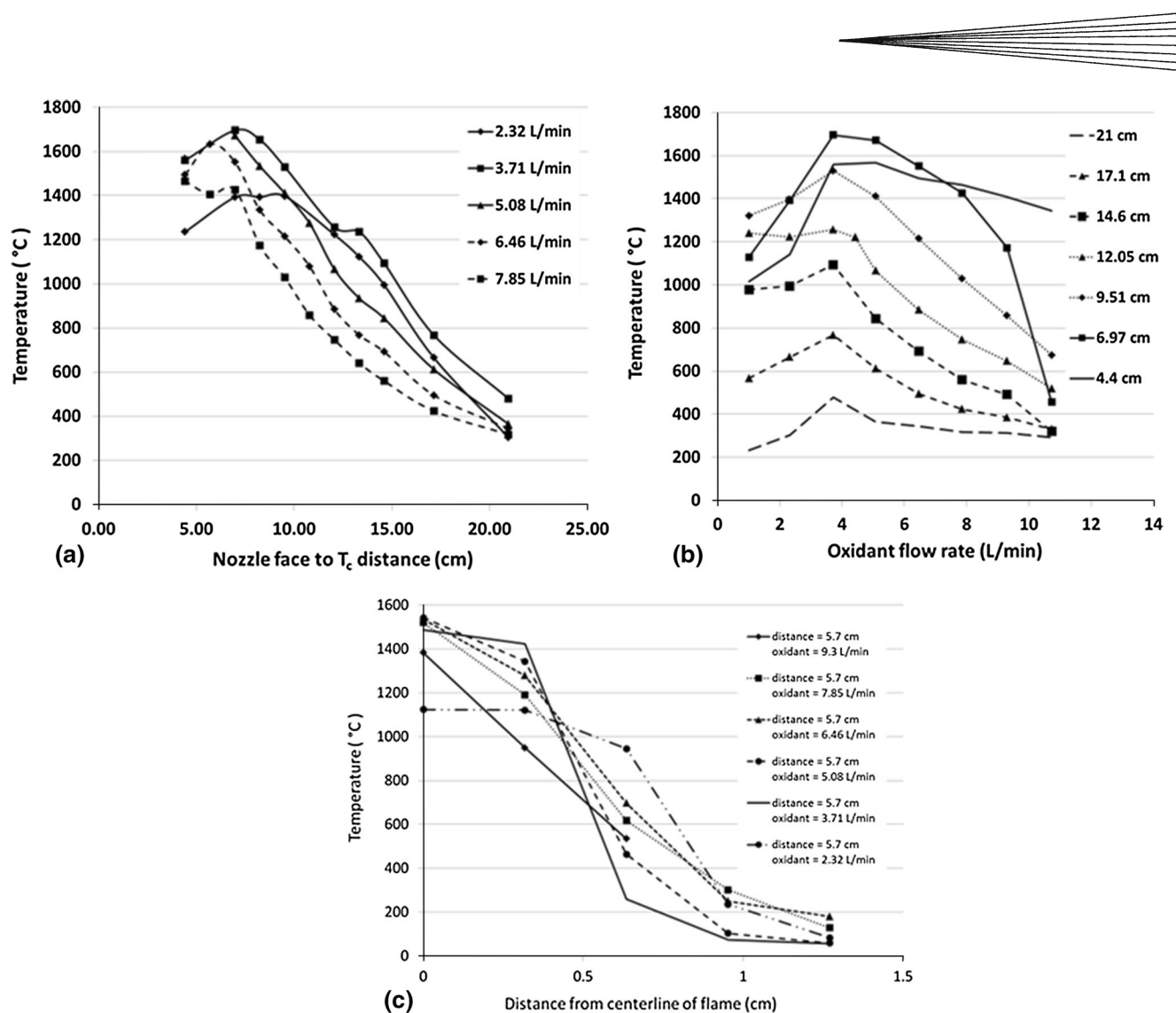
Fig. 9 Temperature profile of the flame as recorded by a Type B Pt-Rh thermocouple as a function of the (a) axial distance from the atomizing burner face, (b) O_2 flow rate, and (c) radial distance from the flame centerline

(Ref 45). This emission could conceivably be used to quickly assess or monitor the fuel/oxidant stoichiometry under a given set of processing conditions.

3.3.4 Flame Temperature Profiles as a Function of Oxidant Flow Rates. In Fig. 9(a), some interesting features of the combustion process are revealed. First, the peak temperature is similar for O_2 flow rates of 3.71, 5.08, and 6.46 L/min at around 1620-1650 °C with the distinction that the location of the peak moves to lower distances with increasing O_2 flow rate due to a faster burning rate (Ref 39, 44). This is another indication of better mixing of fuel and O_2 which leads to an increased burn rate. This increased rate moves the peak temperature (hence complete droplet evaporation) to a location earlier in the reaction zone. This has implications on nanoparticle formation and size uniformity (Ref 46). The temperature profile for 3.71 L/min is the highest over that longest axial distance and this is congruent with the observation that this is the longest flame (Fig. 9a). Second, above 6.46 L/

min, the peak temperature drops indicating cooling from the excess O_2.

Figure 9(b) is a plot of the temperature profile along constant axial sampling locations as a function of O_2 flow rate. Again the temperature increases moving closer to the reaction zone (lower distance). In all plots up to 6.97 cm, the temperature increases to a peak near ~3.7 L/min and then drops with O_2 flow rate; however, at 6.97 and 4.4 cm, the temperature reaches a plateau indicating that the influences of flame length have been attenuated. At these axial locations between an O_2 flow rates of 3.7 and ~6 L/min, the temperature is approximately constant up to the stoichiometric point. This trend occurs once the probe is sampling the most intense reaction zone. Figure 9(c) again shows the very steep radial temperature gradients observed at the edge of the flame. At 3.71 L/min, the gradient is the most uniform across the centerline but above 0.5 cm drops the fastest.

Lower O_2 flow rates result in lower overall flame temperature but a broader and more uniform temperature

across the centerline. Above 5 L/min, the radial temperature gradient gets steeper with increasing O_2 flow rate indicating the strong mixing that confines the reaction toward the centerline. The mixing eliminates the need for O_2 diffusion into the flame (for complete combustion), and thus, the reaction zone does not spread outward as a function of the O_2 gradient.

4. Conclusions

The RSDT process converts metal-organic precursors into metals and metal-oxide coatings. The conversion process can be broken into several stages to facilitate careful study of the fluid dynamics, heat transfer, mass transfer, and combustion. The results of this study indicate that the fuel chemistry and the level of mixing between the fuel and oxidant are crucial to obtaining a fully developed and stable flame. The oxidant flow rate is extremely important in determining the rate of combustion, length of the flame zone, mixing characteristics, velocity, and atomization.

The oxidant flow rate can be tuned to create large or small nanoparticles. For instance, in Pt-based oxygen reduction catalysis (e.g., on the cathode side of a fuel cell), the objective is to have small (3-5 nm) non-agglomerated and dispersed Pt particles. In order to achieve this particle morphology, the fuel must be mixed adequately to form a turbulent diffusion flame. The flame must not create conditions where unwanted Pt coarsening cannot occur, i.e., a long flame with poor mixing. At a fuel flow rate of 4 mL/min for Pt-(acac)$_2$, an O_2 flow rate of 5-7 L/min gives the best mixing without excess cooling or inefficient use of O_2 (a cost driver for the process). In addition, the highest temperature is achieved closer to the atomizing burner under these conditions. This creates the conditions for a uniform nanoparticle formation pathway. Additionally, the length of the flame (and hence residence time) could be controlled by decreasing the area of the annulus between the fuel and O_2 flow. This would affect both atomization and mixing.

Larger nanoparticles, such as in battery cathode materials, are necessary where surface area reactions with the electrolyte should be minimized while still providing adequate pathways for Li$^+$ intercalation. In order to favor larger particles, a longer flame and longer residence time are needed. This could be achieved by reducing the oxidant flow rate (allowing for coagulation and sintering) and/or adding a shroud to limit entrained air.

Future studies will link the processing parameters of propane content, O_2 flow rate, and fuel flow rate to Pt particle size distribution and ultimately to electrochemical behavior.

Acknowledgment

References

1. S.E. Pratsinis, Flame Aerosol Synthesis of Ceramic Powders, *Prog. Energy Combust. Sci.*, 1998, **24**(3), p 197-219
2. W.Y. Teoh, R. Amal, and L. Madler, Flame Spray Pyrolysis: An Enabling Technology for Nanoparticles Design and Fabrication, *Nanoscale*, 2010, **2**(8), p 1324-1347
3. L. Mädler, H.K. Kammler, R. Mueller, and S.E. Pratsinis, Controlled Synthesis of Nanostructured Particles by Flame Spray Pyrolysis, *J. Aerosol Sci.*, 2002, **33**(2), p 369-389
4. R. Strobel, A. Baiker, and S.E. Pratsinis, Aerosol Flame Synthesis of Catalysts, *Adv. Powder Technol.*, 2006, **17**(5), p 457-480
5. R. Strobel and S.E. Pratsinis, Flame Aerosol Synthesis of Smart Nanostructured Materials, *J. Mater. Chem.*, 2007, **17**(45), p 4743-4756
6. H.K. Kammler, L. Mädler, and S.E. Pratsinis, Flame Synthesis of Nanoparticles, *Chem. Eng. Technol.*, 2001, **24**(6), p 583-596
7. R. Strobel and S. Pratsinis, Flame Synthesis of Supported Platinum Group Metals for Catalysis and Sensors, *Platin. Met. Rev.*, 2009, **53**(1), p 11-20
8. M.S. Wooldridge, Gas-Phase Combustion Synthesis of Particles, *Prog. Energy Combust. Sci.*, 1998, **24**(1), p 63-87
9. J. Roller, R. Neagu, F. Orfino, and R. Maric, Supported and Unsupported Platinum Catalysts Prepared by a One-Step Dry Deposition Method and their Oxygen Reduction Reactivity in Acidic Media, *J. Mater. Sci.*, 2012, **47**(11), p 4604-4611
10. J.M. Roller, M.J. Arellano-Jiménez, H. Yu, R. Jain, C.B. Carter, and R. Maric, Catalyst Nanoscale Assembly from the Vapor Phase on Corrosion Resistant Supports, *Electrochim. Acta*, 2013, **107**, p 632-655
11. J. Roller, J. Renner, H. Yu, C. Capuano, T. Kwak, Y. Wang, C.B. Carter, K. Ayers, W.E. Mustain, and R. Maric, Flame-Based Processing as a Practical Approach for Manufacturing Hydrogen Evolution Electrodes, *J. Power Sources*, 2014, **271**, p 366-376
12. F.O. Ernst, R. Büchel, R. Strobel, and S.E. Pratsinis, One-Step Flame-Synthesis of Carbon-Embedded and -Supported Platinum Clusters, *Chem. Mater.*, 2008, **20**(6), p 2117-2123
13. B. Buesser and S.E. Pratsinis, Design of Aerosol Coating Reactors: Precursor Injection, *Ind. Eng. Chem. Res.*, 2011, **50**(24), p 13831-13839
14. B. Buesser and S.E. Pratsinis, Design of Aerosol Particle Coating: Thickness, Texture and Efficiency, *Chem. Eng. Sci.*, 2010, **65**(20), p 5471-5481
15. B. Weidenhof, M. Reiser, K. Stöwe, W.F. Maier, M. Kim, J. Azurdia, E. Gulari, E. Seker, A. Barks, and R.M. Laine, High-Throughput Screening of Nanoparticle Catalysts made by Flame Spray Pyrolysis as Hydrocarbon/NO Oxidation Catalysts, *J. Am. Chem. Soc.*, 2009, **131**(26), p 9207-9219
16. G. Skandan, N. Glumac, Y. Chen, F. Cosandey, E. Heims, and B.H. Kear, Low-pressure Flame Deposition of Nanostructured Oxide Films, *J. Am. Ceram. Soc.*, 1998, **81**(10), p 2753-2756
17. R.C. Breitkopf, J. Hwang, F. Maniei, and A. Hunt, Carbon Supported Pt Nanomaterials for Fuel Cell Applications Using Combustion Chemical Vapor Condensation, *NSTI Nanotech 2003 Conference Technical Program Abstract*, 2003, p 490-492
18. A.T. Hunt, W.B. Carter, and J.K. Cochran, Combustion Chemical Vapor Deposition: A Novel Thin-Film Deposition Technique, *Appl. Phys. Lett.*, 1993, **63**(2), p 266-268
19. I.D. Choi, H. Lee, Y. Shim, and D. Lee, A One-Step Continuous Synthesis of Carbon-Supported Pt Catalysts Using a Flame for the Preparation of the Fuel Electrode, *Langmuir*, 2010, **26**(13), p 11212-11216
20. A. Hunt, Microcoating Technologies Inc., Materials and Processes for Providing Fuel Cells and Active Membranes, Patent US6403245 B1, 11 June 2002
21. A. Hunt, G. Deshpande, T.J. Hwang, M. Oljaca, S. Shanmugham, S. Shoup, et al., Chemical Vapor Deposition Methods for Making
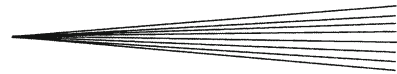
Powders and Coatings, and Coatings Made Using these Methods, Patent US20020058143 A1, 16 May 2002

22. J.M. Roller, M.J. Arellano-Jiménez, R. Jain, H. Yu, C. Barry Carter, and R. Maric, Oxygen Evolution During Water Electrolysis from Thin Films Using Bimetallic Oxides of Ir-Pt and Ir-Ru, *J. Electrochem. Soc.*, 2013, **160**(6), p F716-F730

23. G. Hu, R. Neagu, Q. Wang, Z. Zhang, G. Li, and Y. Zheng, Mathematical Modeling of Flow and Heat/Mass Transfer During Reactive Spraying Deposition Technology (RSDT) Process for High Temperature Fuel Cells, *Eng. Appl. Comput. Fluid Mech.*, 2012, **6**(1), p 134

24. V. Yang, Modeling of Supercritical Vaporization, Mixing, and Combustion Processes in Liquid-Fueled Propulsion Systems, *Proc. Combust. Inst.*, 2000, **28**(1), p 925-942

25. I. Glassman, *Combustion*, Academic Press, Inc., New York, 1977

26. M.T. Swihart, Vapor-Phase Synthesis of Nanoparticles, *Curr. Opin. Colloid Interface Sci.*, 2003, **8**(1), p 127-133

27. S.E. Pratsinis and S. Vemury, Particle Formation in Gases: A Review, *Powder Technol.*, 1996, **88**(3), p 267-273

28. D.E. Rosner, Flame Synthesis of Valuable Nanoparticles: Recent Progress/Current Needs in Areas of Rate Laws, Population Dynamics, and Characterization, *Ind. Eng. Chem. Res.*, 2005, **44**(16), p 6045-6055

29. A. Camenzind, W.R. Caseri, and S.E. Pratsinis, Flame-Made Nanoparticles for Nanocomposites, *Nano Today*, 2010, **5**(1), p 48-65

30. R. Mueller, H.K. Kammler, S.E. Pratsinis, A. Vital, G. Beaucage, and P. Burtscher, Non-Agglomerated Dry Silica Nanoparticles, *Powder Technol.*, 2004, **140**(1-2), p 40-48

31. G.M. Faeth, Evaporation and Combustion of Sprays, *Prog. Energy Combust. Sci.*, 1983, **9**(1-2), p 1-76

32. A. Duvvur, C.H. Chiang, and W.A. Sirignano, Oscillatory Fuel Droplet Vaporization—Driving Mechanism for Combustion Instability, *J. Propul. Power*, 1996, **12**(2), p 358-365

33. A. Lefebvre, *Atomization and Sprays*, Taylor & Francis Group, Boca Raton, 1989

34. N. Syred and J.M. Beér, Combustion in Swirling Flows: A Review, *Combust. Flame*, 1974, **23**(2), p 143-201

35. T. Plessing, C. Kortschik, N. Peters, M.S. Mansour, and R.K. Cheng, Measurements of the Turbulent Burning Velocity and the Structure of Premixed Flames on a Low-Swirl Burner, *Proc. Combust. Inst.*, 2000, **28**(1), p 359-366

36. J.C. Lasheras, A. Fernandez-Pello, and F.L. Dryer, Experimental Observations on the Disruptive Combustion of Free Droplets of Multicomponent Fuels, *Combust. Sci. Technol.*, 1980, **22**(5-6), p 195-209

37. W.Y. Teoh, A Perspective on the Flame Spray Synthesis of Photocatalyst Nanoparticles, *Materials*, 2013, **6**(8), p 3194

38. A.J. Gröhn, S.E. Pratsinis, A. Sánchez-Ferrer, R. Mezzenga, and K. Wegner, Scale-Up of Nanoparticle Synthesis by Flame Spray Pyrolysis: the High-Temperature Particle Residence Time, *Ind. Eng. Chem. Res.*, 2014, **53**(26), p 10734-10742

39. W.R. Hawthorne, D.S. Weddell, and H.C. Hottel, Mixing and Combustion in Turbulent Gas Jets, *Symp. Combust. Flame Explos. Phenom.*, 1949, **3**(1), p 266-288

40. S.J. Brookes and J.B. Moss, Predictions of Soot and Thermal Radiation Properties in Confined Turbulent Jet-Diffusion Flames, *Combust. Flame*, 1999, **116**(4), p 486-503

41. W.A. Sirignano, Fuel Droplet Vaporization and Spray Combustion Theory, *Prog. Energy Combust. Sci.*, 1983, **9**(4), p 291-322

42. B. Abramzon and W.A. Sirignano, Droplet Vaporization Model for Spray Combustion Calculations, *Int. J. Heat Mass Transf.*, 1989, **32**(9), p 1605-1618

43. A. Teleki, B. Buesser, M.C. Heine, F. Krumeich, M.K. Akhtar, and S.E. Pratsinis, Role of Gas-Aerosol Mixing During In Situ Coating of Flame-Made Titania Particles, *Ind. Eng. Chem. Res.*, 2009, **48**(1), p 85-92

44. M.C. Heine, L. Mädler, R. Jossen, and S.E. Pratsinis, Direct Measurement of Entrainment During Nanoparticle Synthesis in Spray Flames, *Combust. Flame*, 2006, **144**(4), p 809-820

45. A. Gaydon, *The Spectroscopy of Flames*, Chapman and Hall, London, 1974

46. S. Tsantilis, H. Briesen, and S.E. Pratsinis, Sintering Time for Silica Particle Growth, *Aerosol Sci. Technol.*, 2001, **34**(3), p 237-246